

Kepler asteroseismology of red-giant stars

Jørgen Christensen-Dalsgaard^{1,2}

¹*Department of Physics and Astronomy, Aarhus University, Ny
Munkegade, 8000 Aarhus C*

²*High Altitude Observatory, National Center for Atmospheric Research,
P.O. Box 3000, Boulder, CO 80307, USA*

Abstract. The *Kepler* mission, launched in March 2009, has revolutionized asteroseismology, providing detailed observations of thousands of stars. This has allowed in-depth analysis of stars ranging from compact hot subdwarfs to red giants, and including the detection of solar-like oscillations in hundreds of stars on or near the main sequence. Here I mainly consider solar-like oscillations in red giants, where *Kepler* observations are yielding results of a perhaps unexpected richness. In addition to giving a brief overview of the observational and numerical results for these stars, I present a simple analysis which captures some of the properties of the observed frequencies.

1. Introduction

High-precision photometry from space is emerging as an extremely important astrophysical tool, particularly in two areas: asteroseismology and the search for extra-solar planets using the transit technique. The small Canadian MOST satellite (e.g., Walker et al. 2003) has shown the way, providing very interesting results on stellar oscillations but also, remarkably, detecting the transit of a planet of just twice the size of the Earth in orbit around a star of magnitude 6 (Winn et al. 2011). The CoRoT mission (e.g., Baglin et al. 2009) was designed with the dual purpose of asteroseismology and exo-planet research. The mission, launched in late 2006, has been highly successful in both areas. The results include the detection of solar-like oscillations in several main-sequence stars (e.g., Michel et al. 2008) and the detection of a ‘super-earth’ with a radius around $1.7 R_{\oplus}$ and a mass around $5 M_{\oplus}$ (e.g., Léger et al. 2009; Queloz et al. 2009).

The *Kepler* mission (Borucki et al. 2009) uses a telescope with a diameter more than three times as big as that of CoRoT. Also, unlike CoRoT which is in a low-Earth orbit, *Kepler* is in an Earth-trailing heliocentric orbit and hence is able to observe the same field almost continuously throughout the mission. The main goal of the mission is to characterize extra-solar planets, particularly planets of roughly earth-size in the habitable zone. This is done through photometric detection of transits of a planet in front of the host star. The transit detections of exo-planet candidates must be followed up by extensive additional analyses and observations to eliminate possible false positives (e.g., Brown 2003). To ensure satisfactory detection statistics *Kepler* continuously observes around 150,000

stars in a field of 110 square degrees in the Cygnus-Lyra region. Further details on the spacecraft and mission were provided by Koch et al. (2010).

The mission was launched in March 2009 and has been spectacularly successful. Amongst the remarkable results have been the statistics of a large number of exo-planet candidates (Borucki et al. 2011), the detection of the first confirmed rocky exo-planet (Batalha et al. 2011) and the detection of a system with 6 planets, with masses determined from the planet-planet interactions (Lissauer et al. 2011).

The photometric requirements of the detection of the transit of an Earth-size planet in front of a star like the Sun, with a reduction in intensity of around 10^{-4} , make the mission ideally suited for asteroseismology. This has led to the establishment of the *Kepler* Asteroseismic Investigation (KAI, Christensen-Dalsgaard et al. 2008). Most objects are observed at a cadence of around 30 min, but a subset of up to 512 stars, the selection of which can be changed on a monthly basis, are observed at a one-minute cadence. A large fraction of these short-cadence slots have been made available to asteroseismology of stars near the main sequence, while the long-cadence data can be used for asteroseismology of larger and more evolved stars, particularly red giants. To make full use of the huge amount of data from the mission, the Kepler Asteroseismic Science Consortium (KASC)¹ has been set up (Kjeldsen et al. 2010); at the time of writing (September 2011) this has more than 500 members, organized into 13 working groups dealing with different types of objects. The asteroseismic data are made available to the members of the KASC through the Kepler Asteroseismic Science Operations Centre (KASOC) in Aarhus, which also deals with the management and internal refereeing of the papers resulting from the KAI. In the early part of the mission a large number of stars were observed for typically one month each, in a survey phase designed to characterize the properties of stars in the field and select targets for the now ongoing detailed studies of specific objects.

The analysis of the asteroseismic data benefits greatly from additional information about the stars. Basic data for a very large number of stars in the *Kepler* field, obtained from multi-colour photometry, are available in the Kepler Input Catalogue (KIC, Brown et al. 2011). However, extensive efforts are under way to secure more accurate data for selected objects (e.g., Molenda-Żakowicz et al. 2010; Molenda-Żakowicz et al. 2011; Uytterhoeven et al. 2010).

A review of the early *Kepler* asteroseismic results was given by Gilliland et al. (2010), while more recent reviews have been provided by Christensen-Dalsgaard & Thompson (2011) and Christensen-Dalsgaard (2011a,b). Here I give a very brief overview of some of the key findings; also, I discuss in somewhat more detail *Kepler* asteroseismology of red giants, which has turned out to be perhaps the most fascinating area.

2. Properties of stellar oscillations

As a background for the discussion of individual types of stars below, it is probably useful to provide a brief overview of the properties of stellar oscilla-

¹see <http://astro.phys.au.dk/KASC/>.

tions. More detailed expositions have been provided, for example, by Unno et al. (1989), Christensen-Dalsgaard (2004), Aerts et al. (2010) and Christensen-Dalsgaard (2011a).

We consider only small-amplitude adiabatic oscillations of spherically symmetric stars. The dependence of a mode of oscillation on co-latitude θ and longitude ϕ can be written as a spherical harmonic $Y_l^m(\theta, \phi)$, where the degree l provides a measure of the total number of nodal lines on the stellar surface and the azimuthal order m measures the number of nodal lines crossing the equator. In the absence of rotation and other departures from spherical symmetry the frequencies are independent of m . From a physical point of view there are two dominant restoring forces at work: pressure perturbations and gravity working on density perturbations. The former case dominates in acoustic waves and leads to modes of oscillation characterized as p modes, while the latter corresponds to internal gravity waves and leads to modes characterized as g modes.

A very good understanding of the properties of the modes can be obtained from simple asymptotic analysis which in fact turns out to have surprisingly broad applicability in the study of asteroseismically interesting stars. By generalizing an analysis by Lamb (1909), Deubner & Gough (1984) showed that the oscillations approximately satisfy

$$\frac{d^2 X}{dr^2} = -K(r)X ; \quad (1)$$

here r is distance to the centre and $X = c^2 \rho^{1/2} \text{div } \boldsymbol{\delta r}$, where $\boldsymbol{\delta r}$ is the displacement vector, c is the adiabatic sound speed and ρ is density. Also

$$K = \frac{1}{c^2} \left[S_l^2 \left(\frac{N^2}{\omega^2} - 1 \right) + \omega^2 - \omega_{\text{ac}}^2 \right] , \quad (2)$$

ω being the frequency of oscillation, is determined by three characteristic frequencies of the star: the *Lamb frequency* S_l , with

$$S_l^2 = \frac{l(l+1)c^2}{r^2} , \quad (3)$$

the *buoyancy frequency* (or *Brunt-Väisälä frequency*) N ,²

$$N^2 = g \left(\frac{1}{\Gamma_1} \frac{d \ln p}{dr} - \frac{d \ln \rho}{dr} \right) , \quad (4)$$

where g is the local gravitational acceleration, and the *acoustic cut-off frequency* ω_{ac} ,

$$\omega_{\text{ac}}^2 = \frac{c^2}{4H^2} \left(1 - 2 \frac{dH}{dr} \right) , \quad (5)$$

where $H = -(d \ln \rho / dr)^{-1}$ is the density scale height. The properties of a mode are largely determined by the regions in the star where the eigenfunction

²Note the relation of N to convective instability: in convectively unstable regions $N^2 < 0$.

oscillates as a function of r , i.e., where $K > 0$. In regions where $K < 0$ the eigenfunction locally increases or decreases exponentially with r . There may be several oscillatory regions, but typically the amplitude is substantially larger in one of these than in the rest, defining the region where the mode is said to be trapped.

The acoustic cut-off frequency is generally large near the stellar surface and small in the interior. For the low-degree modes relevant here the term in S_l^2 in Eq. (2) is small near the surface, and the properties of the oscillations are determined by the magnitude of ω relative to the atmospheric value of ω_{ac} : when ω is less than ω_{ac} the eigenfunction decreases exponentially in the atmosphere, and the mode is trapped in the stellar interior; otherwise, the mode is strongly damped by the loss of energy through running waves in the atmosphere.

The properties of the oscillations in the stellar interior are controlled by the behaviour of S_l and N (see Fig. 1). In unevolved stars N is typically small compared with the characteristic frequencies of p modes. For these, therefore, $K \simeq (\omega^2 - S_l^2)/c^2$ (neglecting ω_{ac}), and the modes are trapped in the region where $\omega > S_l$ in the outer parts of the star, with a lower turning point, $r = r_t$, such that

$$\frac{c(r_t)}{r_t} = \frac{\omega}{\sqrt{l(l+1)}}. \quad (6)$$

At low degree the cyclic frequencies of p modes approximately satisfy

$$\nu_{nl} = \frac{\omega_{nl}}{2\pi} \simeq \Delta\nu \left(n + \frac{l}{2} + \epsilon \right) - d_{nl} \quad (7)$$

(Vandakurov et al. 1967; Tassoul 1980; Gough 1993); here n is the radial order of the mode,

$$\Delta\nu = \left(2 \int_0^R \frac{dr}{c} \right)^{-1} \quad (8)$$

is the inverse sound travel time across a stellar diameter, R being the surface radius, ϵ is a frequency-dependent phase that reflects the behaviour of ω_{ac} near the stellar surface and d_{nl} is a small correction that in main-sequence stars predominantly depends on the sound-speed gradient in the stellar core. On the other hand, g modes have frequencies below N and typically such that $\omega \ll S_l$ in the relevant part of the star; in this case the modes are trapped in a region defined by $\omega < N$. Here the oscillation *periods* satisfy a simple asymptotic relation:

$$\Pi_{nl} = \frac{2\pi}{\omega_{nl}} \simeq \Delta\Pi_l (n + \epsilon_g) \quad (9)$$

(Vandakurov et al. 1967; Tassoul 1980), where ϵ_g is a phase and

$$\Delta\Pi_l = \frac{2\pi^2}{\sqrt{l(l+1)}} \left(\int_{r_1}^{r_2} N \frac{dr}{r} \right)^{-1}, \quad (10)$$

the integral being over the region where the modes are trapped.

As discussed in Section 4 (see also Bedding, these proceedings) the situation is considerably more complicated in evolved stars with a compact core; this leads

to a high value of g and hence N in the interior of the star, such that modes may have a g-mode character in the deep interior, and a p-mode character in the outer, parts of the star. Such *mixed modes* have a very substantial diagnostic potential.

3. Solar-like oscillations

The solar oscillations are most likely intrinsically damped (Balmforth 1992) and excited stochastically by the turbulent near-surface convection (e.g., Goldreich & Keeley 1977). Thus such oscillations can be expected in all stars with significant outer convection zones (Christensen-Dalsgaard & Frandsen 1983; Houdek et al. 1999). An interesting example is the very recent detection, based on *Kepler* data, of solar-like oscillations in a δ Scuti star (Antoci et al. 2011). The combination of damping and excitation leads to a well-defined, bell-shaped envelope of power with a maximum at a cyclic frequency $\nu_{\max} = \omega_{\max}/2\pi$ which approximately scales as the acoustic cut-off frequency ω_{ac} in the atmosphere (Brown et al. 1991). Assuming adiabatic oscillations in an isothermal atmosphere, this yields

$$\nu_{\max} \propto \omega_{\text{ac}} \propto MR^{-2}T_{\text{eff}}^{-1/2}, \quad (11)$$

where M is the mass, and T_{eff} the effective temperature, of the star. This scaling has substantial observational support (e.g., Bedding & Kjeldsen 2003; Stello et al. 2008), while it is still not fully understood from a theoretical point of view (but see Belkacem et al. 2011). For stars on or near the main sequence the frequencies approximately satisfy the asymptotic relation (7). Here the large frequency separation roughly scales, in accordance with homology scaling, as the square root of the mean stellar density, i.e.,

$$\Delta\nu \propto M^{1/2}R^{-3/2}, \quad (12)$$

although with some departures from strict homology that largely depend on T_{eff} (White et al. 2011). A detailed discussion of the observational properties of solar-like oscillations was provided by Bedding (2011).

In the early phases of the *Kepler* project a survey of potential asteroseismic targets was carried out, each typically observed for one month. This led to the detection of a huge number of main-sequence and subgiant stars showing solar-like oscillations, increasing the number of the known cases by more than a factor of 20, relative to earlier ground-based observations and the observations with the CoRoT mission. As discussed by Chaplin et al. (2011a) this provides information about basic stellar properties, through the application of the scaling laws for ν_{\max} and $\Delta\nu$ (Eqs 11 and 12), yielding a very interesting overview of the distribution, in mass and radius, of stars in the solar neighbourhood. These extensive data also allow a calibration of scaling relations that can be used to predict the detectability of solar-like oscillations for a given star (Chaplin et al. 2011b); this is important for the scheduling of further *Kepler* observations and will, suitably generalized, be very valuable for the definition of other observing campaigns.

A selected set of these stars are now being observed for much longer, to improve the precision and level of detail of the observed frequencies and hence

allow detailed characterization of the stellar properties and internal structure, through fits to the individual observed frequencies. Interesting examples of such analyses were carried out by Metcalfe et al. (2010) and Di Mauro et al. (2011) (see also Di Mauro et al., these proceedings), in both cases for stars evolved somewhat beyond the main sequence where modes of mixed p- and g-mode character provided more sensitive information about the stellar properties (see also Bedding, these proceedings). A very interesting analysis of the diagnostic potentials of mixed modes, based on CoRoT observations, was presented by Deheuvels & Michel (2011).

An important aspect of the asteroseismology of solar-like stars is the application to stars found by *Kepler* to be planet hosts. Here the analysis allows the precise determination of the stellar mass and radius, essential for characterizing the properties of the planets detected through the transit technique and follow-up radial velocity measurements, and determination of the stellar age through model fits to the observed frequencies provides a measure of the age of the planetary system. An early example of such analyses, for the previously known planet host HAT-P-7, was provided by Christensen-Dalsgaard et al. (2010), and asteroseismic results were important for the characterization of the first rocky planet detected outside the solar system, Kepler-10b (Batalha et al. 2011).

4. Asteroseismology of red giants

Perhaps the most striking aspect of *Kepler* asteroseismology has been the study of solar-like oscillations in red-giant stars. These have evolved beyond the phase of central hydrogen burning, developing a helium core surrounded by a thin region, the hydrogen-burning shell, providing the energy output of the star. The core contracts while the outer layers expand greatly, accompanied by a reduction of the effective temperature, until the star reaches and evolves up the Hayashi track, at nearly constant T_{eff} . At the tip of the red-giant branch the temperature in the core reaches around 100 MK, enough to start efficient helium burning. Helium ignition is followed by a readjustment of the internal structure, leading to some reduction in the surface radius, and maintaining the hydrogen-burning shell as a substantial contributor to the total energy output of the star. This central helium-burning phase is rather long-lived, with the stars changing relatively little; in stellar clusters this leads to an accumulation of stars in this phase, which is therefore known as the ‘clump phase’.

A red giant has a very compact core, containing a substantial fraction of the stellar mass, and a very extensive convective envelope. This is reflected in the characteristic frequencies, shown in Fig. 1 for a typical red-giant model. As is clear from the behaviour of the buoyancy frequency N , the outer convective envelope extends over more than 90 % of the stellar radius. The border of the helium core, with a mass of $0.21 M$, is marked by the small local maximum in N near $r = 0.0044R$; the large mass within a small region leads to a very large local gravitational acceleration, causing the huge buoyancy frequency (cf. Eq. 4). At a typical oscillation frequency, marked by the horizontal dotted line, the mode behaves as a p mode in the region outside $r = r_2$, marking the bottom of the outer acoustic cavity, and as a g mode inside $r = r_1$. This causes a mixed character of the modes (see also Bedding, these proceedings).

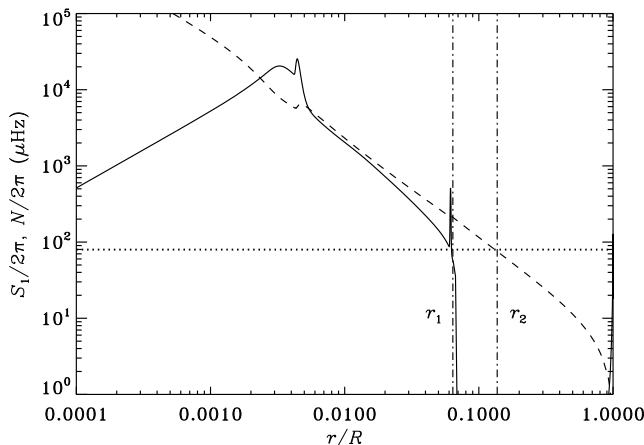


Figure 1. Lamb frequency S_l for $l = 1$ (dashed line) and buoyancy frequency N (solid line), against fractional radius, in a $1 M_\odot$ red-giant model with heavy-element abundance $Z = 0.02$, radius $7 R_\odot$ and luminosity $18.4 L_\odot$. The horizontal dotted line is at $0.7\omega_{\text{ac}}(R)/2\pi$, corresponding roughly to the predicted frequency ν_{max} of maximum power. The vertical dot-dashed lines mark the outer limit r_1 of the g-mode, and the lower limit r_2 of the p-mode, propagating regions at this frequency.

4.1. Properties of red-giant oscillations

Early predictions of solar-like oscillations in red giants were made by Christensen-Dalsgaard & Frandsen (1983). This was followed by detections in ground-based observations (e.g., Frandsen et al. 2002); however, it was only with the CoRoT observations by De Ridder et al. (2009) that the presence of nonradial solar-like oscillations in red giants was definitely established. Very extensive observations of large numbers of stars have been made with both CoRoT and *Kepler* (e.g., Hekker et al. 2009; Bedding et al. 2010; Mosser et al. 2010; Kallinger et al. 2010; Hekker et al. 2011). This has allowed the determination of global stellar properties from fits to the large frequency separation $\Delta\nu$ (cf. Eq. 7) and the frequency ν_{max} at maximum power, possibly supplemented by additional observations in analyses based on stellar model grids, allowing population studies of the red giants (e.g., Miglio et al. 2009, 2011). Particularly interesting are the possibilities for studying the open clusters in the *Kepler* field (Stello et al. 2010, 2011a; Basu et al. 2011). The large number and variety of stars observed have allowed the study of the overall properties of the oscillation frequencies, along the lines of the p-mode asymptotic relation (Eq. 7), (Huber et al. 2010; Mosser et al. 2011a), in what the latter call the universal pattern of the frequencies, and the diagnostic potential of this pattern (Montalbán et al. 2010). Similarly, it has been possible to test scaling relations for mode properties, including their amplitudes, over a broad range of stellar parameters (Huber et al. 2011; Mosser et al. 2011b; Stello et al. 2011b). Di Mauro et al. (2011) demonstrated the diagnostic potential of analysing the individual frequencies in a relatively unevolved red giant, while Jiang et al. (2011) carried out a detailed analysis of a somewhat more evolved star.

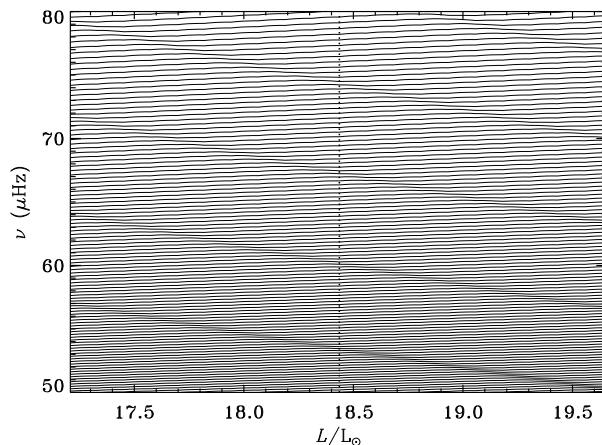


Figure 2. Computed frequencies for a short segment of a $1 M_{\odot}$ evolution sequence, plotted against luminosity in solar units. The age goes from 11.765 to 11.777 Gyr. The vertical dotted line indicates the model illustrated in Figs 1, 4 and 5.

To understand the observed oscillation spectra it is informative to consider in more detail the oscillation properties of red-giant models; here I consider models in the vicinity of the model illustrated in Fig. 1. The huge buoyancy frequency in the core of the model leads to very small g-mode period spacings (cf. Eq. 10): for $l = 1$ the result is $\Delta\Pi_1 = 1.23$ min. The full range of radial modes, up to the acoustical cut-off frequency, extends in cyclic frequency from 11 to $107 \mu\text{Hz}$. In that interval we therefore expect around 1100 g modes of degree $l = 1$, the number scaling like $\sqrt{l(l+1)}/2$ for higher degree.³

Most of these modes have their highest amplitude in the core of the model and hence predominantly have the character of g modes. However, there are frequencies where the eigenfunctions decrease with increasing depth in the region between r_2 and r_1 (cf. Fig. 1). These frequencies define *acoustic resonances* where the modes have their largest amplitude in the outer acoustic cavity and the modes predominantly have the character of p modes.

The properties of the frequencies are illustrated in Fig. 2, showing the evolution of $l = 1$ modes with age, in a relatively limited range in frequency. The extremely high density of modes is evident, as are the branches of acoustic resonances, with frequency decreasing roughly as $R^{-3/2}$, proportional to the mean density of the star. As discussed by Bedding (these proceedings) these undergo avoided crossings with the g modes, whose frequencies increase somewhat with age as the buoyancy frequency in the core increases. The acoustic resonances, together with the frequencies of radial modes, approximately satisfy the asymptotic relation given in Eq. (7).

³This also places heavy constraints on the numerical precision of the calculation of the oscillations. In the numerical calculations illustrated here I used 19,200 mesh points, distributed to match the asymptotic properties of the eigenfunctions, which secured reasonable precision of the results (Christensen-Dalsgaard et al., in preparation).

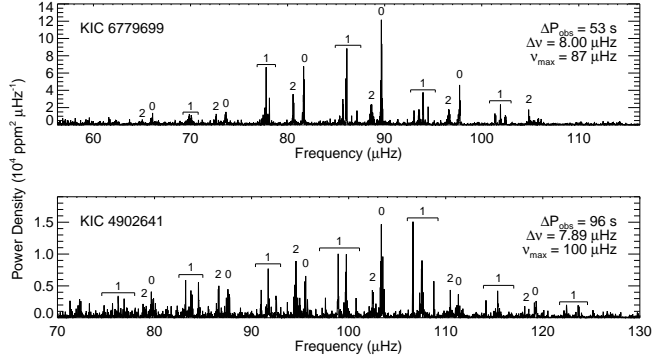


Figure 3. Power spectra of two red giants observed by *Kepler* for 13 and 10 months, respectively; the stars are identified by the Kepler Input Catalog (KIC) numbers. As indicated in the figure, the stars have similar $\Delta\nu$ and ν_{\max} and hence similar overall properties. The horizontal bars marked ‘1’ indicate the dipole forests from which were inferred rather different observed period spacings, ΔP_{obs} , of 52 and 96 s for the upper and lower spectrum. Further analysis determined the asymptotic g-mode spacings as 74 and 147 s, respectively. KIC 6779699 is in the ascending red-giant phase, whereas KIC 4902641 is in the clump phase, with central helium burning. Adapted from Bedding et al. (2011).

A major breakthrough in the asteroseismic study of red giants was the detection of ‘dipole forests’ at the acoustic resonances, i.e., groups of $l = 1$ modes excited to observable amplitudes (Beck et al. 2011; Bedding et al. 2011; Mosser et al. 2011c). These showed an approximately uniform period spacing, as expected for g modes from Eq. (9), and in some cases it was possible from the observed spacings to extrapolate to the period spacing $\Delta\Pi_1$ for the pure g modes. Strikingly, Bedding et al. (2011) demonstrated a substantial difference in the period spacing between stars in the shell hydrogen burning phase and ‘clump stars’ which in addition had core helium burning. This is illustrated in the observed spectra shown in Fig. 3. It was argued by Christensen-Dalsgaard (2011a) that the larger period spacing in the helium-burning stars is a natural consequence of the very temperature-dependent energy generation near the centre in these stars: this leads to a convective core which restricts the range of the integral in Eq. (10), thus reducing its value and hence increasing $\Delta\Pi$.

An important quantity characterizing the properties of the modes is the normalized mode inertia

$$E = \frac{\int_V \rho |\boldsymbol{\delta r}|^2 dV}{M |\boldsymbol{\delta r}_s|^2}, \quad (13)$$

where $\boldsymbol{\delta r}_s$ is the surface displacement, and the integral is over the volume V of the star. Modes of predominantly acoustic nature, including the radial modes, have their largest displacement in the outer parts of the star and hence a relatively low inertia, whereas g-dominated modes have a large amplitude in the deep interior and hence a high inertia. This is illustrated in Fig. 4 for modes of degree $l = 0, 1$ and 2. The acoustic resonances, the inertia decreasing to close to the value for a radial mode of corresponding frequency, are evident, while for the intermediate g-dominated modes the inertia is obviously much higher.

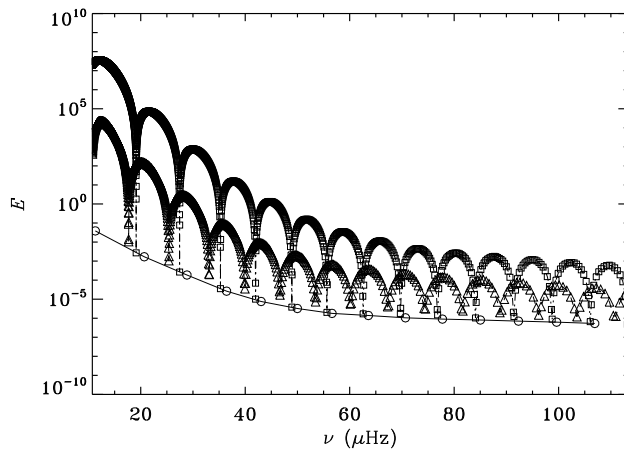


Figure 4. Mode inertias (cf. Eq. 13) for the $1 M_{\odot}$ model illustrated in Fig. 1. Radial modes, with $l = 0$, are shown with circles connected by a line, $l = 1$ modes are shown with triangles and $l = 2$ modes with squares.

On the assumption of damped modes excited stochastically by near-surface convection, the mode inertia is important for understanding the observed amplitudes. A very illuminating discussion of this was provided by Dupret et al. (2009). In the frequent case where the damping is predominantly near the surface, the mode lifetime is proportional to E , with the g-dominated modes having lifetimes of years. Also, the mean square amplitude is inversely proportional to E . However, the visibility of the modes in the power spectrum is determined with the *peak height* which under these circumstances is independent of E , assuming observations extending for substantially more than the mode lifetimes (see also Chaplin et al. 2005). The present observations are much shorter than the typical lifetimes of the g-dominated modes but still allow several modes to be seen close to the acoustic resonances, particularly for $l = 1$, leading to the dipolar forests of peaks.

As noted by Beck et al. (2011) and Bedding et al. (2011) the signature of modes affected by the g-mode behaviour is an approximately uniform period spacing. This is illustrated for the model in Fig. 5. For the bulk of the modes, which are predominantly g modes, the spacing is close to the asymptotic value, indicated by the horizontal dashed line. Near the acoustic resonances the avoided crossings cause a reduction in the period spacing, of a characteristic 'V'-shaped pattern. This is closely related to the behaviour of the mode inertia, illustrated in figure by the scaled mode inertia $Q_{nl} = E_{nl}/\bar{E}_0(\omega_{nl})$ where $\bar{E}_0(\omega_{nl})$ is the inertia of the radial modes, interpolated to the frequency ω_{nl} of the mode considered.

4.2. A simple asymptotic analysis

To understand the properties of the modes it is useful to illustrate them with a crude approximation to the asymptotic description provided by Eqs (1) and (2). We neglect ω_{ac}^2 whose main effect is to ensure reflection of the mode at the stellar surface; this causes a phase shift which can easily be included. From the behaviour of the characteristic frequencies illustrated in Fig. 1 we can

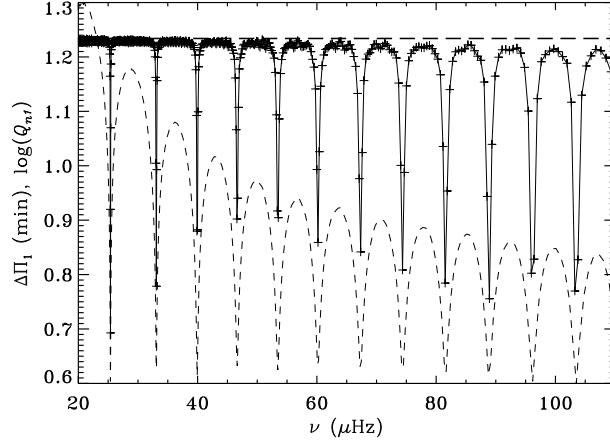


Figure 5. The pluses connected by solid lines show period spacings for modes with $l = 1$ in the $1 M_{\odot}$ model illustrated in Fig. 1. The heavy horizontal dashed line shows the asymptotic period spacing (cf. Eq. 10). The thin dashed curve shows, on an arbitrary scale, the logarithm of the mode inertia divided by the inertia of radial modes (see text).

approximately divide the star into three regions, separated at $r = r_1$ and r_2 (see figure):

1. $r < r_1$: here $S_l^2 \gg \omega^2$ and $N^2 \gg \omega^2$, except near the turning points. Here we approximate K by

$$K \simeq \frac{l(l+1)}{r^2} \left(\frac{N^2}{\omega^2} - 1 \right) \simeq \frac{l(l+1)}{r^2} \frac{N^2}{\omega^2}, \quad (14)$$

where the last approximation is valid except near the turning points where $\omega = N$.

2. $r_1 < r < r_2$: here $S_l^2 \gg \omega^2 \gg N^2$. Thus K is simply approximated by

$$K \simeq -\frac{l(l+1)}{r^2}. \quad (15)$$

3. $r_2 < r$: Here $N^2 \ll \omega^2$ and $S_l^2 \ll \omega^2$ except near the turning point where $\omega = S_l$. Thus we approximate K by

$$K \simeq \frac{1}{c^2} (\omega^2 - S_l^2) \simeq \frac{\omega^2}{c^2}, \quad (16)$$

where the last approximation is valid except near the turning point.

With these approximations we can write down the solutions in the different regions based on the JWKB approximation, neglecting, however, the details of the behaviour near the turning points.⁴ In region 1) the solution can be written

⁴These can be treated with a proper JWKB analysis (e.g., Gough 2007); the effect, however, would essentially just be to change the phases of the solution, with no qualitative change in the behaviour found here.

as

$$X(r) \simeq A^{(g)}(r) \cos(\Psi^{(g)}(r) + \phi^{(g)}) , \quad (17)$$

where

$$\Psi^{(g)} = \int_0^r \frac{L}{r'} \frac{N}{\omega} dr' , \quad (18)$$

with $L = \sqrt{l(l+1)}$, and $\phi^{(g)}$ is a phase that depends on the behaviour near the centre and the turning points. In region 2) the approximate solution is simply

$$X(r) \simeq a_+ \left(\frac{r}{r_1} \right)^L + a_- \left(\frac{r}{r_1} \right)^{-L} , \quad (19)$$

where a_+ and a_- are integration constants determined by fitting the solutions. Finally, in region 3) the solution can be written as

$$X(r) \simeq A^{(p)}(r) \cos(\Psi^{(p)}(r) + \phi^{(p)}) , \quad (20)$$

where

$$\Psi^{(p)} = \int_r^R \omega \frac{dr'}{c} , \quad (21)$$

and $\phi^{(p)}$ is a phase that depends on the behaviour near the surface (thus including the contribution from the reflection caused by ω_{ac}) and the turning point. In Eqs (17) and (20) the amplitude functions $A^{(g)}(r)$ and $A^{(p)}(r)$ can be obtained from the JWKB analysis; since they are irrelevant for the subsequent analysis, I do not present them explicitly.

The full solution is obtained by requiring continuity of X and dX/dr at r_1 and r_2 . Neglecting the derivatives of $A^{(g)}(r)$ and $A^{(p)}(r)$ this yields

$$\begin{aligned} & \sin(\Psi^{(g)}(r_1) + \phi^{(g)} - \pi/4) \sin(\Psi^{(p)}(r_2) + \phi^{(p)} - \pi/4) + \\ & \zeta \cos(\Psi^{(g)}(r_1) + \phi^{(g)} - \pi/4) \cos(\Psi^{(p)}(r_2) + \phi^{(p)} - \pi/4) = 0 , \end{aligned} \quad (22)$$

where $\zeta = (r_1/r_2)^{2L}$ is a measure of the coupling between regions 1) and 3). If $\zeta = 0$, so that the regions are completely decoupled, the eigenfrequencies obviously satisfy

$$\Psi^{(g)}(r_1) = \int_0^{r_1} \frac{L}{r} \frac{N}{\omega} dr = n\pi - \tilde{\phi}^{(g)} , \quad (23)$$

or

$$\Psi^{(p)}(r_2) = \int_{r_2}^R \omega \frac{dr}{c} = k\pi - \tilde{\phi}^{(p)} , \quad (24)$$

where n and k are integers and $\tilde{\phi}^{(g)} = \phi^{(g)} - \pi/4$, $\tilde{\phi}^{(p)} = \phi^{(p)} - \pi/4$. Equation (23) leads to Eqs (9) and (10), while Eq. (24) essentially corresponds to Eq. (7), taking into account that the behaviour near the lower turning point leads to the dependence on l .⁵

⁵For purely acoustic modes extending over the whole star, this follows from an analysis of the oscillations near the centre (e.g., Gough 1993). In the present case of a red giant, where the lower turning point is in a region outside the compact core, this behaviour is in fact not fully understood.

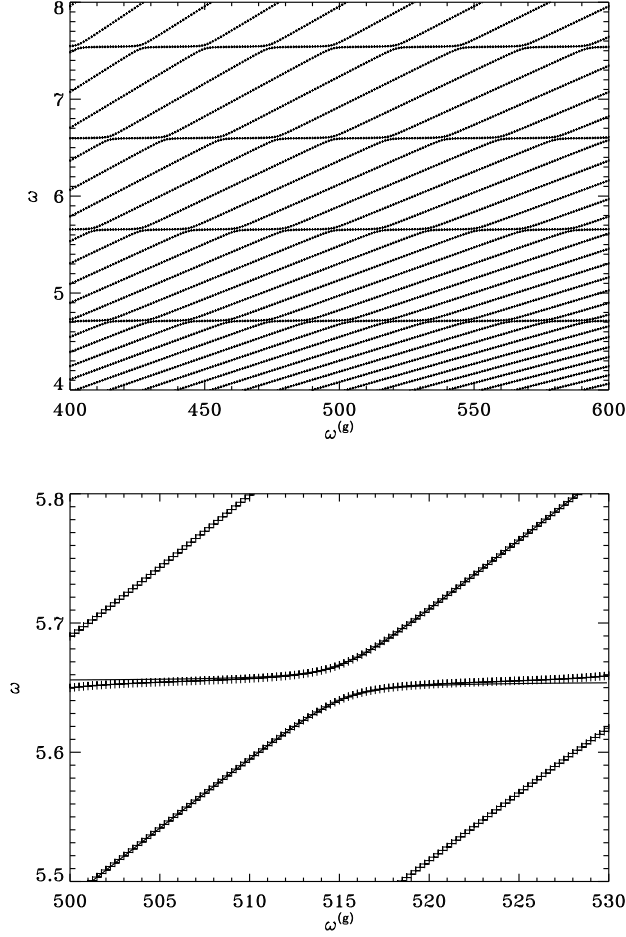


Figure 6. The upper panel shows solutions to the dispersion relation in Eq. (25), as a function of $\omega^{(g)}$, keeping $\omega^{(p)} = 0.3$ and $\zeta = 0.01$ fixed. The lower panel shows a small segment of the solution; the solid curves show the approximate solution near the avoided crossing, given by Eq. (29).

To analyse the full dispersion relation, Eq. (22), we neglect the dependence of the turning points r_1 and r_2 on frequency and write the relation as

$$\mathcal{D} = \sin(\omega^{(g)}/\omega + \tilde{\phi}^{(g)}) \sin(\omega/\omega^{(p)} + \tilde{\phi}^{(p)}) + \zeta \cos(\omega^{(g)}/\omega + \tilde{\phi}^{(g)}) \cos(\omega/\omega^{(p)} + \tilde{\phi}^{(p)}) = 0, \quad (25)$$

with⁶

$$\omega^{(g)} = L \int_0^{r_1} \frac{N}{r} dr, \quad \omega^{(p)} = \left(\int_{r_2}^R \frac{dr}{c} \right)^{-1}. \quad (26)$$

To illustrate the properties of the solution, Fig. 6 shows the result of increasing $\omega^{(g)}$, keeping $\omega^{(p)}$ fixed; for simplicity I assume that $\tilde{\phi}^{(g)} = \tilde{\phi}^{(p)} = 0$. It is obvious

⁶Since the integral in Eq. (8) is dominated by the outer layers, $\omega^{(p)} \simeq 2\Delta\nu$.

that the increase in $\omega^{(g)}$ leads to avoided crossings between frequencies satisfying Eq. (23), increasing with $\omega^{(g)}$, and the constant frequencies satisfying Eq. (24). Details of an avoided crossing are shown in the lower panel of Fig. 6. At the corresponding crossing of the uncoupled modes, we have both $\omega \equiv \omega_c = k\pi\omega^{(p)}$ and $\omega^{(g)}/\omega_c = n\pi$ for suitable integers k and n ; thus the crossing is defined by $\omega^{(g)} \equiv \omega_c^{(g)} = nk\pi^2$. With

$$\omega^{(g)} = \omega_c^{(g)} + \delta\omega^{(g)} , \quad \omega = \omega_c + \delta\omega , \quad (27)$$

and expanding Eq. (25) to second order in $\delta\omega$, $\delta\omega^{(g)}$ and ζ we obtain

$$\delta\omega^2 - \frac{\omega_c}{\omega_c^{(g)}} \delta\omega^{(g)} \delta\omega - \zeta \frac{\omega_c^2 \omega^{(p)}}{\omega_c^{(g)}} = 0 , \quad (28)$$

with the solution

$$\delta\omega = \frac{1}{2} \frac{\omega_c}{\omega_c^{(g)}} \delta\omega^{(g)} \pm \left[\frac{1}{4} \left(\frac{\omega_c}{\omega_c^{(g)}} \delta\omega^{(g)} \right)^2 + \zeta \frac{\omega_c^2 \omega^{(p)}}{\omega_c^{(g)}} \right]^{1/2} . \quad (29)$$

This is also shown in Fig. 6 for one of the avoided crossings and clearly provides an excellent fit to the numerical solution. The minimum separation between the two branches, for $\delta\omega^{(g)} = 0$, is

$$\Delta\omega_{\min} = 2\omega_c \left(\frac{\omega^{(p)}}{\omega^{(g)}} \right)^{1/2} \zeta^{1/2} . \quad (30)$$

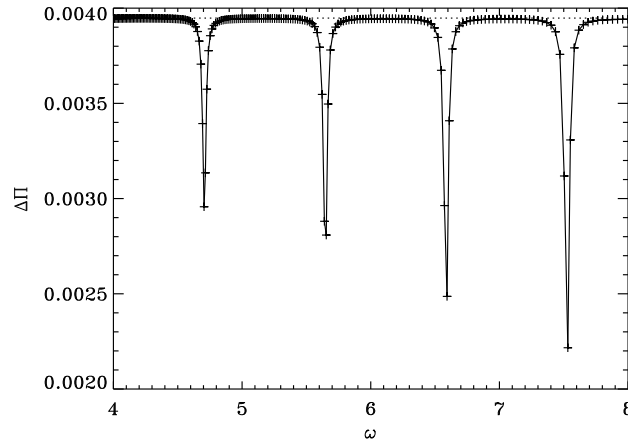


Figure 7. Period spacings for solutions to the asymptotic dispersion relation, Eq. (25), with $\omega^{(p)} = 0.3$, $\omega^{(g)} = 5000$ and $\zeta = 0.04$. The period spacing $2\pi^2/\omega^{(g)}$ for pure g modes is shown by the horizontal dotted line.

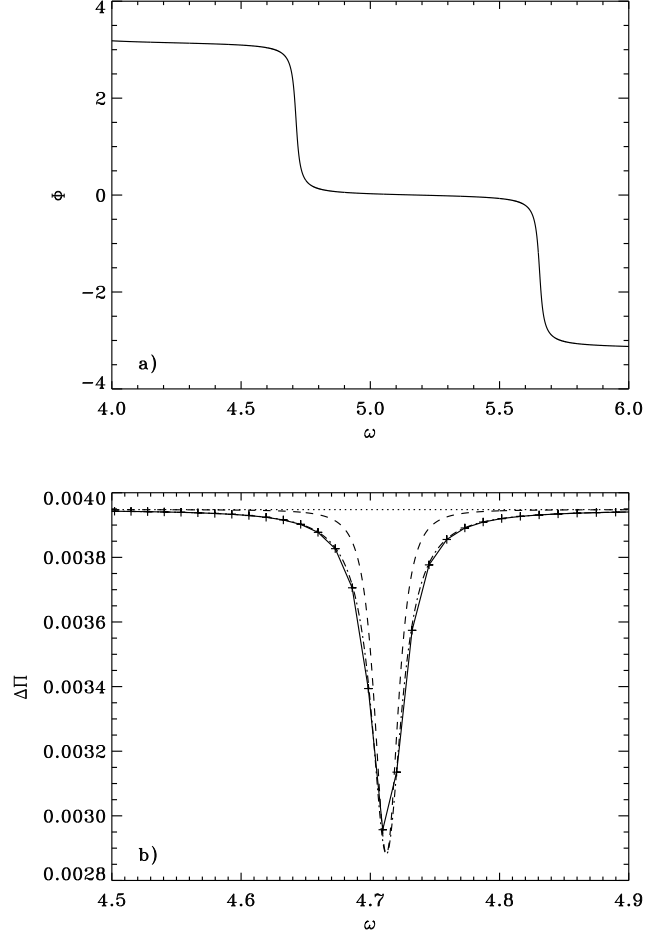


Figure 8. Detailed properties of the case illustrated in Fig. 7. a) The frequency-dependent phase defined by Eq. (32), to within an arbitrary multiple of 2π . b) The pluses and solid curve show a blow-up of Fig. 7. The dot-dashed curve shows the period spacing determined from Eq. (34), using the phase Φ shown in panel a). The dashed curve shows the approximation in Eq. (36).

As in the case of the full solution (cf. Fig. 5) the avoided crossings cause dips in the otherwise uniform period spacings. This is illustrated in Fig. 7. To understand this behaviour in more detail we write Eq. (25) as

$$\mathcal{D} = C(\omega) \sin(\omega^{(\text{g})}/\omega + \Phi(\omega)) , \quad (31)$$

where (assuming again $\tilde{\phi}^{(\text{g})} = \tilde{\phi}^{(\text{p})} = 0$) $C(\omega) = \sqrt{\sin^2(\omega/\omega^{(\text{p})}) + \zeta^2 \cos^2(\omega/\omega^{(\text{p})})}$ and $\Phi(\omega)$ satisfies

$$\begin{aligned} C(\omega) \cos(\Phi) &= \sin(\omega/\omega^{(\text{p})}) \\ C(\omega) \sin(\Phi) &= \zeta \cos(\omega/\omega^{(\text{p})}) . \end{aligned} \quad (32)$$

It is obvious that the eigenfrequencies satisfy

$$\mathcal{G}(\omega) = \omega^{(\text{g})}/\omega + \Phi(\omega) = n\pi , \quad (33)$$

for integer n . Φ is illustrated in Fig. 8a; except near acoustic resonances, where $\omega/\omega^{(\text{p})} \simeq k\pi$ for integer k , Φ is almost constant and the period spacing is determined by the first term in \mathcal{G} , essentially corresponding to the pure g-mode case defined by Eq. (23). Near the acoustic resonances Φ changes rapidly, causing a strong variation in the period spacing.

This behaviour can be made more precise by noting that the frequency spacing between adjacent modes approximately satisfies $\Delta\omega \simeq \pi(d\mathcal{G}/d\omega)^{-1}$ and hence the period spacing is, approximately, given by

$$\Delta\Pi \simeq -\frac{2\pi^2}{\omega^2} \left(\frac{d\mathcal{G}}{d\omega} \right)^{-1} = \frac{2\pi^2/\omega^{(\text{g})}}{1 - \frac{\omega^2}{\omega^{(\text{g})}} \frac{d\Phi}{d\omega}} . \quad (34)$$

Here the numerator is the period spacing for pure g modes, and the denominator causes a reduction in $\Delta\Pi$ near an acoustic resonance. This is illustrated in Fig. 8b where the actual period spacings near an acoustic resonance are compared with Eq. (34).

At the centre of an acoustic resonance $\omega/\omega^{(\text{p})} = k\pi$ and $\Phi = \pi/2$, up to an irrelevant multiple of π . In the vicinity of this point we can expand Φ as $\delta\Phi = \Phi - \pi/2$ in terms of $\delta x = \omega/\omega^{(\text{p})} - k\pi$, to obtain

$$\delta\Phi \simeq -\frac{\delta x}{\sqrt{\zeta^2 + \delta x^2}} , \quad (35)$$

and hence the period spacing

$$\Delta\Pi \simeq \frac{2\pi^2/\omega^{(\text{g})}}{1 + \frac{\omega^2}{\omega^{(\text{g})}\omega^{(\text{p})}} \frac{\zeta^2}{(\zeta^2 + \delta x^2)^{3/2}}} . \quad (36)$$

This approximation is also shown in Fig. 8b. In particular, we obtain the minimum period spacing

$$\Delta\Pi_{\text{min}} \simeq \frac{2\pi^2/\omega^{(\text{g})}}{1 + \frac{\omega^2}{\zeta\omega^{(\text{g})}\omega^{(\text{p})}}} . \quad (37)$$

It is interesting that the maximum reduction in the period spacing increases with decreasing ζ and hence weaker coupling. On the other hand, the width of the decrease in $\Delta\Pi$ also decreases and so therefore do the chances of finding a g mode in the vicinity of the minimum.

Although the present analysis is highly simplified (and consequently quite simple), it does appear to capture many of the aspects of the numerical solutions for stellar models. It would probably not be difficult to generalize it to take the behaviour near the turning points properly into account, making reasonable a more detailed comparison with the numerical results. A comparison with the behaviour of the mode inertia (Fig. 4) would similarly have been interesting. Such efforts are beyond the scope of the present paper, however. I also note that there is clearly some symmetry between the treatment of the g- and p-dominated modes in how the frequency-dependent phase function Φ is introduced. In the present case, with a dense spectrum of g modes undergoing avoided crossings with a smaller number of p modes, it was natural to regard the effect of the latter as a modification, in terms of Φ , to the dispersion relation for the former. For subgiants, on the other hand, with a comparatively dense spectrum of p modes and few g modes, a similar phase could be introduced in the p-mode dispersion relation. This might be interesting in connection with the analysis presented by Bedding (these proceedings).

5. Future prospects

It is obvious that *Kepler* has already been an overwhelming success, resulting in observations that will be analysed for years to come. Even so, it is crucial to ensure that the mission continues beyond the nominal end in late 2012. For the exo-planet research this is required to reach the planned sensitivity to Earth-like planets, given a stellar background noise that has been found to be somewhat higher than expected. For asteroseismology the gains will be numerous. A longer mission will allow further searches for rare types of oscillating stars, exemplified by the recent detection in the *Kepler* field of an oscillating white dwarf (Østensen et al. 2011). The possibilities for detecting frequency variations associated with stellar cycles in solar-like stars (Karooff et al. 2009) will be much improved. Also, longer timeseries will allow reaching further peaks, for modes with longer lifetimes, in the dipolar forests in red giants and hence greatly strengthen the possibilities for investigating the properties of their cores.

However, there is clearly a need to consider observational facilities beyond *Kepler*. The proposed ESA PLATO mission (Catala et al. 2011) for transit search for exo-planets would allow asteroseismic characterization of a large fraction of the stars where planet systems are detected; in addition, it would cover a much larger area on the sky than *Kepler*, and hence provide a greater variety of asteroseismic targets.⁷ Also, ground-based observations of stellar oscillations in radial velocity still present great advantages over the photometric observations by *Kepler*. This is particularly important for solar-like stars, where the

⁷Regrettably, PLATO failed to get selected in October 2011; it remains to be seen whether it will enter into the competition for a later selection.

‘noise’ from other processes in the stellar atmosphere provides a background that is much higher, relative to the oscillations, in intensity than in Doppler velocity (Harvey 1988; Grundahl et al. 2007). This is the background for establishing the SONG⁸ network (Christensen-Dalsgaard 2011b; Grundahl et al. 2011) of one meter telescopes, with a distribution to ensure almost continuous observations anywhere in the sky. The first node in the network, built largely with Danish funding, will start operations in 2012, a Chinese node is under construction, and partners are being sought to establish additional nodes.

Acknowledgments. I wish to express my deep sympathy with the Japanese people for the losses sustained in the disaster immediately preceding this conference. I am very grateful to the organizers for carrying through, in these difficult circumstances, with the conference, with great success and in beautiful surroundings. I thank Tim Bedding for providing Fig. 3, and Travis Metcalfe and Dennis Stello for comments on earlier versions of the manuscript. NCAR is supported by the National Science Foundation.

References

- Aerts, C., Christensen-Dalsgaard, J. & Kurtz, D. W. 2010, *Asteroseismology*, (Heidelberg: Springer)
- Antoci, V., Handler, G., Campante, T. L., et al. 2011, *Nature*, 477, 570
- Baglin, A., Auvergne, M., Barge, P., Deleuil, M., Michel, E. and the CoRoT Exoplanet Science Team 2009, in *Proc. IAU Symp. 253, Transiting Planets*, edited by F. Pont, D. Sasselov and M. Holman, (Cambridge: IAU and Cambridge University Press), 71
- Balmforth, N. J. 1992, *MNRAS*, 255, 603
- Basu, S., Grundahl, F., Stello, D., et al. 2011, *ApJ*, 729, L10
- Batalha, N. M., Borucki, W. J., Bryson, S. T., et al. 2011, *ApJ*, 729, 27
- Beck, P. G., Bedding, T. R., Mosser, B., et al. 2011, *Science*, 332, 205.
- Bedding, T. R. 2011, to appear in *Asteroseismology, Canary Islands Winter School of Astrophysics, Volume XXII*, edited by P. L. Pallé, (Cambridge: Cambridge University Press) [[arXiv:1107.1723](#)]
- Bedding, T. R., Huber, D., Stello, D., et al. 2010, *ApJ*, 713, L176
- Bedding, T. R. & Kjeldsen, H. 2003, *PASA*, 20, 203
- Bedding, T. R., Mosser, B., Huber, D., et al. 2011, *Nature*, 471, 608
- Belkacem, K., Goupil, M. J., Dupret, M. A., Samadi, R., Baudin, F., Noels, A. & Mosser, B. 2011, *A&A*, 530, A142
- Borucki, W. J., Koch, D. G., Basri, G., et al. 2011, *ApJ*, 736, 19
- Borucki, W., Koch, D., Batalha, N., Caldwell, D., Christensen-Dalsgaard, J., Cochran, W. D., Dunham, E., Gautier, T. N., Geary, J., Gilliland, R., Jenkins, J., Kjeldsen, H., Lissauer, J. J. & Rowe, J. 2009, in *Proc. IAU Symp. 253, Transiting Planets*, edited by F. Pont, D. Sasselov and M. Holman, (Cambridge: IAU and Cambridge University Press), 289
- Brown, T. M. 2003, *ApJ*, 593, L125
- Brown, T. M., Gilliland, R. L., Noyes, R. W. & Ramsey, L. W. 1991, *ApJ*, 368, 599
- Brown, T. M., Latham, D. W., Everett, M. E. & Esquerdo, G. A. 2011, *AJ*, 142, 112
- Catala, C., Appourchaux, T. and the PLATO Mission Consortium 2011, *J. Phys.: Conf. Ser.*, 271, 012084

⁸Stellar Observations Network Group

- Chaplin, W. J., Houdek, G., Elsworth, Y., Gough, D. O., Isaak, G. R. & New, R. 2005, *MNRAS*, 360, 859
- Chaplin, W. J., Kjeldsen, H., Christensen-Dalsgaard, J., et al. 2011a, *Science*, 332, 213
- Chaplin, W. J., Kjeldsen, H., Bedding, T. R., et al. 2011b, *ApJ*, 732, 54
- Christensen-Dalsgaard, J. 2004, *Solar Phys.*, 220, 137
- Christensen-Dalsgaard, J. 2011a, to appear in *Asteroseismology*, Canary Islands Winter School of Astrophysics, Volume XXII, edited by P. L. Pallé, (Cambridge: Cambridge University Press) [[arXiv:1106.5946](#)]
- Christensen-Dalsgaard, J. 2011b, in *Proc. MEARIM II. The 2nd Middle-East and Africa Regional IAU Meeting*, edited by P. Charles, *African Skies / Cieux Africains*, in the press
- Christensen-Dalsgaard, J. & Frandsen, S. 1983, *Solar Phys.*, 82, 469
- Christensen-Dalsgaard, J. & Thompson, M. J. 2011, in *Proc. IAU Symposium 271: Astrophysical dynamics: from stars to planets*, edited by N. Brummell, A. S. Brun, M. S. Miesch and Y. Ponty, (Cambridge: IAU and Cambridge University Press), 32
- Christensen-Dalsgaard, J., Arentoft, T., Brown, T. M., Gilliland, R. L., Kjeldsen, H., Borucki, W. J. & Koch, D. 2008, *J. Phys.: Conf. Ser.*, 118, 012039
- Christensen-Dalsgaard, J., Kjeldsen, H., Brown, T. M., Gilliland, R. L., Arentoft, T., Frandsen, S., Quirion, P.-O., Borucki, W. J., Koch, D. & Jenkins, J. M. 2010, *ApJ*, 713, L164
- Deheuvels, S. & Michel, E. 2011, *A&A*, in the press [[arXiv:1109.1191v1](#)]
- De Ridder, J., Barban, C., Baudin, F., et al. 2009, *Nature*, 459, 398
- Deubner, F.-L. & Gough, D. O. 1984, *ARA&A*, 22, 593
- Di Mauro, M. P., Cardini, D., Catanzaro, G., et al. 2011, *MNRAS*, 415, 3783
- Dupret, M.-A., Belkacem, K., Samadi, R., Montalbán, J., Moreira, O., Miglio, A., Godart, M., Ventura, P., Ludwig, H.-G., Grigahcène, A., Goupil, M.-J., Noels, A. & Caffau, E. 2009, *A&A*, 506, 57
- Frandsen, S., Carrier, F., Aerts, C., Stello, D., Maas, T., Burnet, M., Bruntt, H., Teixeira, T. C., de Medeiros, J. R., Bouchy, F., Kjeldsen, H., Pijpers, F. & Christensen-Dalsgaard, J. 2002, *A&A*, 394, L5
- Gilliland, R. L., Brown, T. M., Christensen-Dalsgaard, J., et al. 2010, *PASP*, 122, 131
- Goldreich, P. & Keeley, D. A. 1977, *ApJ*, 212, 243
- Gough, D. O. 1993, in *Astrophysical fluid dynamics*, Les Houches Session XLVII, edited by J.-P. Zahn and J. Zinn-Justin, (Amsterdam: Elsevier), 399
- Gough, D. O. 2007, *AN*, 328, 273
- Grundahl, F., Kjeldsen, H., Christensen-Dalsgaard, J., Arentoft, T. & Frandsen, S. 2007, *Comm. in Asteroseismology*, 150, 300
- Grundahl, F., Christensen-Dalsgaard, J., Jørgensen, U. G., Kjeldsen, H., Frandsen, S. & Kjærgaard Rasmussen, P. 2011, *J. Phys.: Conf. Ser.*, 271, 012083
- Harvey, J. W. 1988, in *Proc. IAU Symposium No 123, Advances in helio- and asteroseismology*, edited by J. Christensen-Dalsgaard and S. Frandsen, (Dordrecht: Reidel), 497
- Hekker, S., Kallinger, T., Baudin, F., De Ridder, J., Barban, C., Carrier, F., Hatzes, A. P., Weiss, W. W. & Baglin, A. 2009, *A&A*, 506, 465
- Hekker, S., Gilliland, R. L., Elsworth, Y., Chaplin, W. J., De Ridder, J., Stello, D., Kallinger, T., Ibrahim, K. A., Klaus, T. C. & Li, J. 2011, *MNRAS*, 414, 2594
- Houdek, G., Balmforth, N. J., Christensen-Dalsgaard, J. & Gough, D. O. 1999, *A&A*, 351, 582
- Huber, D., Bedding, T. R., Stello, D., et al. 2010, *ApJ*, 723, 1607
- Huber, D., Bedding, T. R., Stello, D., et al. 2011, *ApJ*, in the press [[arXiv:1109.3460](#)]
- Jiang, C., Jiang, B. W., Christensen-Dalsgaard, J., et al. 2011, *ApJ*, in the press [[arXiv:1109.0962](#)]
- Kallinger, T., Mosser, B., Hekker, S., et al. 2010, *A&A*, 522, A1

- Karoff, C., Metcalfe, T. S., Chaplin, W. J., Elsworth, Y., Kjeldsen, H., Arentoft, T. & Buzasi, D. 2009, *MNRAS*, 399, 914
- Kjeldsen, H., Christensen-Dalsgaard, J., Handberg, R., Brown, T. M., Gilliland, R. L., Borucki, W. J. & Koch, D. 2010, *AN*, 331, 966
- Koch, D. G., Borucki, W. J., Basri, G., et al. 2010, *ApJ*, 713, L79
- Lamb, H. 1909, *Proc. London Math. Soc.*, 7, 122
- Léger, A., Rouan, D., Schneider, J., et al. 2009, *A&A*, 506, 287
- Lissauer, J. J., Fabrycky, D. C., Ford, E. B., et al. 2011, *Nature*, 470, 53
- Metcalfe, T. S., Monteiro, M. J. P. F. G., Thompson, M. J., et al. 2010, *ApJ*, 723, 1583
- Michel, E., Baglin, A., Auvergne, M., et al. 2008, *Science*, 322, 558
- Miglio, A., Montalbán, J., Baudin, F., Eggenberger, P., Noels, A., Hekker, S., De Ridder, J., Weiss, W. & Baglin, A. 2009, *A&A*, 503, L21
- Miglio, A., Brogaard, K., Stello, D., et al. 2011, *MNRAS*, in the press [[arXiv:1109.4376](#)].
- Molenda-Żakowicz, J., Bruntt, H., Sousa, S., et al. 2010, *AN*, 331, 981
- Molenda-Żakowicz, J., Latham, D. W., Catanzaro, G., Frasca, A. & Quinn, S. N. 2011, *MNRAS*, 412, 1210
- Montalbán, J., Miglio, A., Noels, A., Scuflaire, R. & Ventura, P. 2010, *ApJ*, 721, L182
- Mosser, B., Belkacem, K., Goupil, M.-J., et al. 2010, *A&A*, 517, A22
- Mosser, B., Belkacem, K., Goupil, M. J., et al. 2011a, *A&A*, 525, L9
- Mosser, B., Elsworth, Y., Hekker, S., et al. 2011b, *A&A*, in the press [[arXiv:1110.0980v1](#)]
- Mosser, B., Barban, C., Montalbán, J., et al. 2011c, *A&A*, 532, A86
- Østensen, R. H., Bloemen, S., Vučković, M., Aerts, C., Oreiro, R., Kinemuchi, K., Still, M. & Koester, D. 2011, *ApJ*, 736, L39
- Queloz, D., Bouchy, F., Moutou, C., et al. 2009, *A&A*, 506, 303
- Stello, D., Bruntt, H., Preston, H. & Buzasi, D. 2008, *ApJ*, 674, L53
- Stello, D., Basu, S., Bruntt, H., et al. 2010, *ApJ*, 713, L182
- Stello, D., Meibom, S., Gilliland, R. L., et al. 2011a, *ApJ*, 739, 13
- Stello, D., Huber, D., Kallinger, T., et al. 2011b, *ApJ*, 737, L10
- Tassoul, M. 1980, *ApJS*, 43, 469
- Unno, W., Osaki, Y., Ando, H., Saio, H. & Shibahashi, H. 1989, *Nonradial Oscillations of Stars*, 2nd Edition (Tokyo: University of Tokyo Press)
- Uytterhoeven, K., Briquet, M., Bruntt, H., et al. 2010, *AN*, 331, 993
- Vandakurov, Yu. V. 1967, *AZh*, 44, 786 (English translation: *Soviet Ast.*, 11, 630)
- Walker, G., Matthews, J., Kuschnig, R., et al. 2003, *PASP*, 115, 1023
- White, T. R., Bedding, T. R., Stello, D., Christensen-Dalsgaard, J., Huber, D. & Kjeldsen, H. 2011, *ApJ*, in the press [[arXiv:1109.3455](#)]
- Winn, J. N., Matthews, J. M., Dawson, R. I., et al. 2011, *ApJ*, 737, L18